Molecular-dynamics simulation of silicon clusters

Estela Blaisten-Barojas
Instituto de Física, Universidad Nacional Autónoma de México, Apartado Postal 20-364, 01000 México Distrito Federal, México

D. Levesque
Laboratoire de Physique Théorique et Hautes Energies, Université de Paris—Sud, 91405 Orsay Cédex, France
(Received 19 March 1986)

A molecular-dynamics simulation of 10- to 32-silicon-atom clusters was carried out using the potential of Stillinger and Weber [Phys. Rev. B **31**, 5262 (1985)] including two- and three-atom contributions. Both neutral and positively charged clusters were examined to determine their corresponding minimum-energy configurations. The cluster-growth sequence is obtained with these cluster configurations which resulted from quenches of each equilibrated N-atom cluster configuration at finite temperatures to low temperature. Cooling and heating experiments were carried out up to temperatures of about 1500 K showing that the solid-liquid phase transition is smeared in these isolated small clusters. Analysis of the pair correlation function $g(r)$ and of the density distribution of angles between bonds offer a convenient way to observe the local order in these small systems.

I. INTRODUCTION

The structural characteristics of covalent noncrystalline solids have been discussed from different viewpoints. It is recognized that such systems have short-range order without exact symmetry elements. The study of disordered systems has led, for example, to theories such as statistical geometry[1] where a prescription of topological properties allows the construction of an infinite network with statistical distributions of its metrical properties.[2] A less explored approach is that of searching for a class of potential functions[3,4] to model covalent materials and predict details of the aggregation process that yield local defects associated with amorphous structures.[1,5] This last approach can also be of interest in the description of the growth of "individual" stable conformations of covalent clusters condensed out of the vapor at low temperatures.

Recent mass spectrometric experiments on Si^+ (Refs. 6 and 7), Ge^+ (Ref. 7), and Sn^+ (Ref. 7) clusters show trends toward overlapping series of most prominent cluster sizes specially in the $(Si)_n^+$ case. Martin and Shaber[7] have recognized the importance of some kind of topological reconnection of the bonds in an aggregate by suggesting the possibility that 5-silicon-atom rings are the buildings blocks of certain amorphous types of cluster growth. This possibility has also been stated[5] in a computer simulation experiment of silicon condensed phases when studying the local structure of defects that aggregate in the crystalline medium upon annealing.

For silicon and the covalent materials, pair potentials alone are insufficient to describe the equilibrium diamond lattice. Several potentials including two- and three-body terms have been used in the literature[4] to compute structural energies of covalent crystals. In particular the Stillinger and Weber[5] (SW) potential has nine parameters that were adjusted to fit the silicon properties of condensed phases such as bond length, cohesive energy, melting temperature, to satisfy qualitatively the Lindemann melting criterion for solids and to reproduce the property of shrinking when silicon melts. The purpose of this contribution is to explore the way in which the SW classical potential model is adequate for the description of the initial stages of growth of neutral and charged silicon clusters.

The organization of the paper is as follows. In Sec. II an outline of the SW nonadditive interaction potential is given as well as a description of the modification of this interaction that results when an atom becomes positively charged in each cluster. Details of the molecular dynamics simulation are also given in order to describe a series of annealing computer experiments for 8- to 17- and 32-atom clusters. Section III focuses on the resulting sequences of growth obtained for both neutral and charged clusters. The structural properties are discussed in Sec. IV and the paper is concluded in Sec. V.

II. MODEL AND METHODS

The interaction among N identical atoms with coordinates $(\mathbf{r}_1,\mathbf{r}_2,\ldots,\mathbf{r}_N)$ can be expanded into n-body contributions as follows:

$$V(\mathbf{r}_1,\mathbf{r}_2,\ldots,\mathbf{r}_N)=\sum_{i=1}^{N} v_1(\mathbf{r}_i)+\sum_{\substack{i<j\\ i,j=1}}^{N} v_2(\mathbf{r}_i,\mathbf{r}_j)+\sum_{\substack{i<j<k\\ i,j,k=1}}^{N} v_3(\mathbf{r}_i,\mathbf{r}_j,\mathbf{r}_k)+\cdots+\sum_{\substack{i_1,i_2,\ldots,i_n=1\\ i_1<i_2<\cdots<i_n}}^{N} v_n(\mathbf{r}_{i_1},\mathbf{r}_{i_2},\ldots,\mathbf{r}_{i_n})+\cdots . \quad (1)$$

It is usually believed that this series is rapidly convergent and that the first three terms give a reasonable approximation to the interaction potential. Without external fields, the SW potential contains only pair and triplet terms of the form:[5]

$$v_2(r)=\begin{cases}A(Br^{-p}-r^{-q})\exp[(r-a)^{-1}], & r<a\\ 0, & r\geq a\end{cases} \tag{2}$$

and

$$v_3(r_{ij},r_{ik},r_{jk})=h(r_{ij},r_{ik},\theta_{jik})+h(r_{ji},r_{jk},\theta_{ijk})+h(r_{ki},r_{kj},\theta_{ikj}) , \tag{3}$$

where θ_{jik} is the angle subtended between j and k at vertex i for any triplet of atoms and the function h is given by

$$h(r_{ij},r_{ik},\theta_{jik})=\lambda\exp[\gamma(r_{ij}-a)^{-1}+\gamma(r_{ik}-a)^{-1}]\times(\cos\theta_{jik}+\tfrac{1}{3})^2 . \tag{4}$$

This function vanishes unless both $r_{ij}<a$ and $r_{ik}<a$. Therefore the range of interaction between atoms has a finite cutoff ratio at $r=a$. The choice of the nine parameters in this work is the same as used in Ref. (5), namely, $A=7.049\,556\,227$, $B=0.602\,224\,558\,4$, $p=4$, $q=0$, $a=1.8$, $\lambda=21.0$, and $\alpha=1.2$. All values are given in reduced units of $\sigma=2.0951$ Å for distances and $\varepsilon=2.167$ eV/atom pair for energies.

Consider next that one of the atoms of the cluster, say atom number 1 is ionized. The electric field which results from the positive charge q of this atom induces dipole moment $\boldsymbol{\mu}_j$ on the $N-1$ atoms of the cluster. If the polarizability α of the atoms is considered as isotropic, then the energy U^{ind} added by the charge to the cluster energy V is

$$U^{\text{ind}}=-q\sum_{i=2}^{N}\boldsymbol{\mu}_i\cdot\frac{\mathbf{r}_{i1}}{r_{i1}}+\sum_{\substack{i,j=1\\ i>j}}^{N}\boldsymbol{\mu}_i\cdot\overleftrightarrow{\mathrm{T}}\cdot\boldsymbol{\mu}_j+\sum_{i=1}^{N}\frac{\boldsymbol{\mu}_i^2}{2\alpha} , \tag{5}$$

where $\overleftrightarrow{\mathrm{T}}$ is the dipole tensor $\nabla\nabla(1/r)$.

In the present work the contribution of the induced dipole $\boldsymbol{\mu}_j$ to the electric field on the clusters atoms was neglected. Only the linear terms in α were kept leading to $\boldsymbol{\mu}_j=-q\alpha\mathbf{r}_{j1}/r_{j1}^3$ and such that

$$U^{\text{ind}}\equiv\sum_{j=2}^{N}V_1(\mathbf{r}_j)\equiv-\tfrac{1}{2}\sum_{j=2}^{N}q^2\frac{\alpha}{r_{1j}^4} . \tag{6}$$

Higher-order terms in α could have been included in U^{ind}, but since Eq. (6) is to be added to the SW model potential containing both pair additive and nonadditive contributions, extra terms in U^{ind} might as well result in a different choice of the nine parameters. Equation (6) is a realization of augmenting the model potential function with single-particle terms $v_1(r_j)$ which reproduces approximately the interaction between an ionized atom with all other atoms in the cluster. This situation of ionized clusters should be closer to the mass spectra experiments. Thus, for charged clusters, the total potential energy V is given by the three first terms of Eq. (1). The first term corresponds to Eq. (6) and the components of the second and third term to Eqs. (2)–(4). The molecular dynamics simulations were performed with this potential energy, where q equals zero for neutral clusters and $-q$ equals one electronic charge for ionized clusters.

Molecular dynamics at constant energy was used throughout; units of length and energy were chosen to be σ and ε. Reduced quantities were adopted for distance, temperature, energy, and time: $r^*=r/\sigma$, $T^*=kT/\varepsilon$, $V^*=V/\varepsilon$, and $t^*=t/\tau$, where $\tau=(m\sigma^2/\varepsilon)^{1/2}=7.66\times10^{-14}$ s and m is the silicon atom mass. A reference density of $\rho_0^*=0.46\sigma^{-3}$ was chosen equal to the bulk value. The equations of motion were solved using the Verlet algorithm[8] with a time step of $\Delta t^*=0.01$ which yields good energy conservation.

A "cluster" is defined as that aggregate of N atoms held together by the interaction energy described in the above paragraphs. Since the range of interaction between atoms has a finite cutoff radius a, a configuration of atoms is kept as a "cluster" if the atoms on the cluster surface are at distances from their nearest neighbors smaller than a. Whenever the kinetic energy of an atom is large enough to push it outside the cutoff, the simulation is stopped since the cluster is "evaporating." This last condition restricts the study to clusters at low temperature.

Various annealing and quenching experiments were carried out in the following way. First, an initial configuration is chosen and the cluster equilibrated at the highest possible temperature consistent with its definition. Second, the clusters are cooled at rates $\Delta T^*/\Delta t^*\simeq5\times10^{-3}$ down to zero temperature. Third, the clusters are led through a cycle of reheating followed by cooling to $T^*=0$ to assure that the system is not trapped in a metastable state at zero temperature. Typically, runs at each temperature step last 20τ, allowing 5τ for equilibration followed by an averaging time of 15τ.

III. BINDING ENERGY AND SEQUENCES OF CLUSTER GROWTH

Figures 1(a) and 1(b) show some molecular dynamics results for the mean potential energy per particle $\langle V^*\rangle/N$ as a function of reduced temperature T^*. Figure 1(a) corresponds to neutral cluster in Eq. (6), whereas Fig. 1(b) gives the results obtained for charged clusters with $q=1$ and $\alpha=7.2$ Å^3.[9] The behavior of the mean potential energy displayed in the figure does not show any variation reminiscent of the bulk silicon first-order phase change at $T^*=0.08$.[5] This is an indication that under the SW model potential even $N=32$ is not a sufficiently large number of atoms to demonstrate a sharp phase transition. However, it should be mentioned, that other classes of potential functions[10,11] show a smeared phase transition for clusters as small as $N=13$. Although Fig. 1 shows no transition, it is pertinent to say that the dispersion of points for $T^*\simeq0.06$ was larger than near the low- and high-temperature regions. Indeed, in Fig. 2 are plotted the results of two selected experiments that might show a phase change. The neutral 15-atom cluster was heated with a slight change of heating rate near $T^*=0.07$; the two paths obtained are shown in Fig. 2(a). Among other

cooling experiments performed on the positively charged 14-atom cluster, in Fig. 2(b) is shown a fairly clear smooth discontinuity of $\langle V^* \rangle / N$ near $T^* \simeq 0.07$. Since for other cluster sizes it was not possible to extract a clean path, it is risky to advance a final conclusion on the existence of a smeared phase change near $T^* \simeq 0.07$ on the basis of an analysis of the potential energy dependence on temperature.

The low-temperature limit in Fig. 1 seems reliable since it agrees well with the expected equipartition result for harmonic normal modes, namely the reduced constant-volume heat capacity

$$C_v^* = \frac{C_v}{Nk\varepsilon} = \frac{3N-6}{2N} , \tag{7}$$

exactly reproduces the slope of the curves in Fig. 1. The slope in a macroscopic solid is known to increase to 2 as a result of anharmonic interactions. In these clusters the increase seems to be somewhat larger, ~ 2.5, probably due to large anharmonic amplitudes of oscillation of the surface atoms.

The $T^* \to 0$ limit of $|\langle V^* \rangle / N|$, defines the binding energy per particle associated with a specific geometrical configuration of atoms. The values of these energies are plotted in Fig. 3 versus N for both neutral and positively charged clusters. These energies were reached by the method described at the end of Sec. II, i.e., by a quenching process where each intermediate state is an equilibrated state of the cluster. The approach is therefore different from other works[4] where certain metastable configurations called amorphous are reached by a mimic of an infinitely fast quench. In fact, many metastable configurations of higher energy can be reached by changing the quenching rate when forming the clusters. Figure 3 shows (dotted line) a sequence of growth that corresponds to the series of symmetric structures built by 4-atom

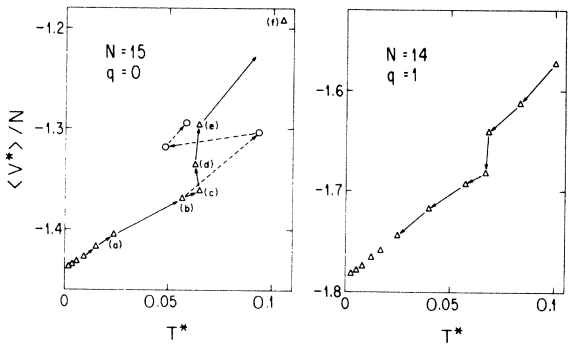

FIG. 2. Mean reduced potential energy per atom as a function of reduced temperature. (a) Heating of the 15-atom cluster following two paths: (i) from (a) through (f); and (ii) from (a) to (b) followed by the dashed line. (b) Cooling path followed by the 14-atom cluster. Potential energy is in units of ε.

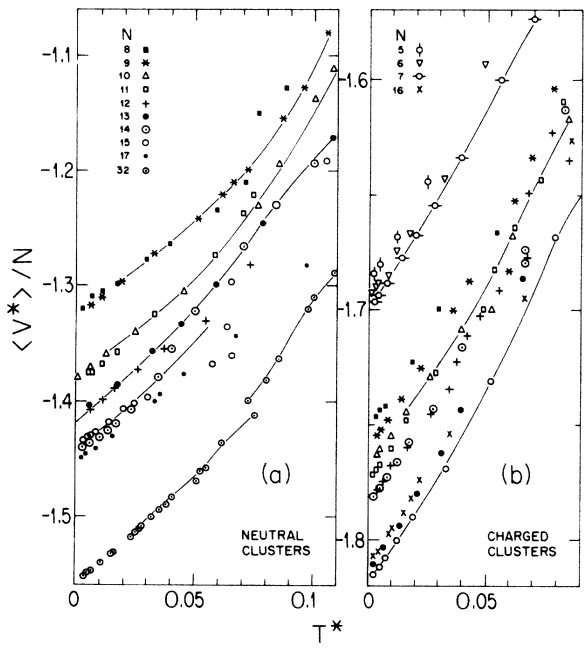

FIG. 1. Mean reduced potential energy per atom as a function of reduced temperature. Molecular-dynamics runs are plotted in (a) for neutral clusters composed of 8 to 17 atoms and 32 atoms; (b) for positively charged clusters composed of 5 to 16 atoms. Potential energy is in units of ε. The lines are drawn to guide the eye.

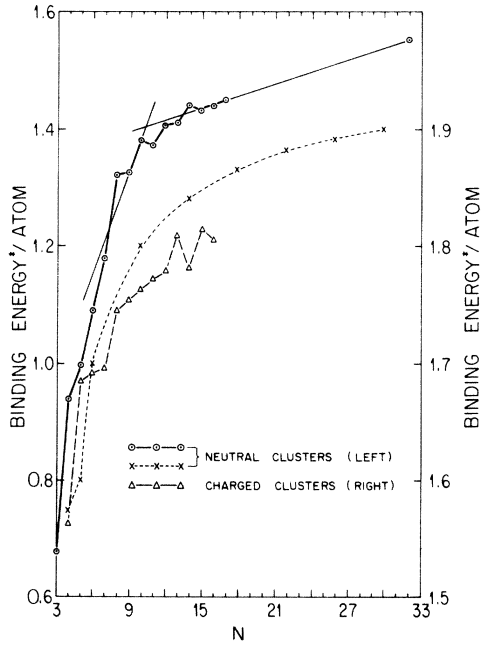

FIG. 3. Reduced binding energy per atom versus the number of atoms in the cluster. Full and dashed lines sketch the dynamically obtained sequence of most stable configurations of neutral and positively charged clusters. Dotted line gives the growth obtained by adding tetrahedrally bonded 4-atom units. Full and dotted lines are drawn with respect to the left scale and dashed line to the right scale.

tetrahedrally bonded units. This sequence should end with the open diamond crystal.[7] It is evident that using the SW potential model the tetrahedral growth corresponds to metastable cluster configurations of lower binding energy, therefore less stable than the sequence of configurations obtained by the previously described quench.

It is tempting to associate the peaks of high binding energy in Fig. 3 to the most abundant clusters observed experimentally in mass spectra. However, as pointed out above, it is possible to draw other sequences of growth corresponding to metastable structures. It is not clear if the experimental conditions are going to favor some of them more than others.[12] In the case resulting from the simulation, it is seen from the $T^*=0$ values of $\langle V^* \rangle/N$ in Fig. 1(a), as well as from the small peaks of the binding energy in Fig. 3, that neutral clusters containing less than 8 atoms are in a region of steady increase of the binding energy, whereas the pairs with (8,9), (10,11), (12,13), (14,15), and (16,17) atoms have almost equal binding energy per particle. There is a slight enhancement of the binding energy for clusters with 10 and 14 atoms. For positively charged clusters [Fig. 1(b) and dashed-line (right) scale in Fig. 3] the binding energy is about the same for the (5,6,7)-, (8,9,10,11,12,14)-, and (13,15,16)-atom clusters with a slight enhancement when $N=13$ and 15.

In close packed materials, it is easy to correlate "magic numbers" (more abundant clusters) to the closing of an atomic shell around a central atom. This is characteristic of materials with high-coordination number (mean number of bonds that each atom is capable of forming). However, when the coordination number is low, as in tetrahedrally bonded materials, this concept of atomic shells is lost. In addition, in the case of isolated aggregates all the atoms tend to be on the cluster surface and therefore the coordination number is about 3. This is shown in Fig. 4, where *bonds* are defined as nearest neighbor distances ≤ 1.4. Clusters with less than 8 atoms (neutral and charged) have average coordination number smaller than 3. As the cluster size increases the coordination number tends slowly toward 4. Notice that the tetrahedral growth implies much lower coordination number with a poor asymptotic behavior (dotted line).

On the other hand, the obtained sequence of growth of maximum binding energy presents a remarkable feature. If one analyzes the slope of the binding energy per atom in Fig. 3, it is evident that a sharp change in the qualitative mechanism of aggregation that takes place at $N \simeq 11$ for neutral clusters. This fact may be correlated with the observation of Martin and Shaber[7] of a well-defined transition from silicon-rich clusters to hydrogen-rich clusters $(SiH)_N^+$ occurring precisely at $N=11$. Clusters smaller than $N=11$ need to add silicon atoms in order to be stable. Clusters larger than $N=11$ have coordination number 3 and will tend to pick up hydrogen atoms, namely one H per Si atom exactly as observed in the experiments. As the cluster increases its size and the coordination number is larger the mass spectrum of Si_NH_x clusters will show a ratio x/N less than one. The Si-H pairs on the surface of the cluster are usually at distances approximately 20% less than the Si-Si. Since H—H bonds are not

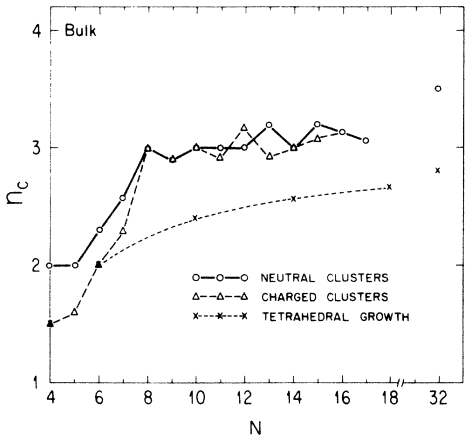

FIG. 4. Mean coordination number as a function of the number of atoms in the cluster. Bonds are neighbor distances $\leq 1.4\sigma$.

to be formed,[13] hydrogens are not likely to change much the previously described conformations of the neutral $(Si)_N$ clusters. Charged $(Si_NH_x)^+$ clusters with $N>11$ probably resemble more the neutral, pure $(Si)_N$ clusters, whereas the $(Si)_N^+$ clusters with $N<11$ are to be regarded as charged.

The geometrical configurations at $T=0$ that result from this simulation are plotted in Fig. 5 for neutral clusters and in Fig. 6 for positively charged clusters. The

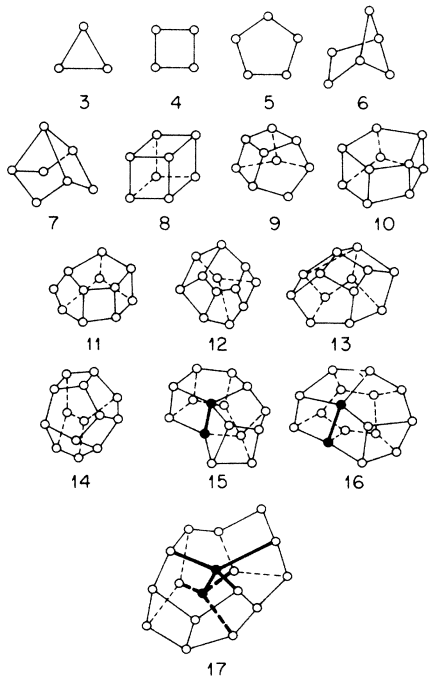

FIG. 5. Sequence of the most stable configurations of neutral clusters at $T^* \cong 0$ as obtained from the molecular-dynamics simulation. Bonded atoms are at distances $\leq 1.4\sigma$.

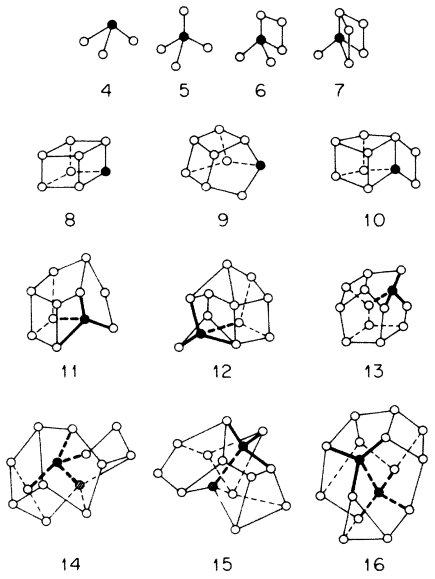

FIG. 6. Sequence of the most stable configurations of positively charged clusters at $T^* \cong 0$ as obtained from the molecular dynamics simulation. Bonded atoms are at distances ≤ 1.4. Black dots correspond to charged atoms.

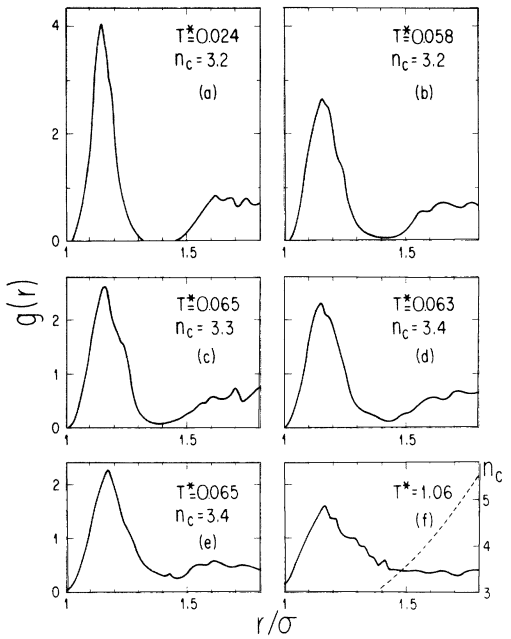

FIG. 7. Pair correlation function of the neutral 15-atom cluster for each of the six temperature steps labeled (a) through (f) in Fig. 2(a).

neutral series was complemented with clusters with $N \leq 7$ whose configurations were obtained by a complete minimization of the cluster potential energy using a quasi-Newton method. The neutral clusters tend to form faces with four and five atoms. However, it is possible internally to connect the vertex atoms by 5-, 6-, 7-, and 8-member rings where each atom is bonded only to two other atoms within the ring. It is interesting to note that only the 6-, 10-, and 14-atom clusters do not allow the formation of 6-member rings. The tetrahedral bonding starts to build up for the 15-atom cluster. There it is evident a distorted 8-atom unit where two members have coordination four (black dots in Fig. 5). Finally, the 17-atom cluster shows an internal 8-member unit of tetrahedral symmetry with a distortion of the dihedral angle adequate to form a boat 6-member ring. The charged series is qualitatively different, the positive charge tends to assume a coordination of four. Therefore distorted five atom tetrahedral units are present very early in the sequence of growth (black dots and thick bonds in Fig. 6). When the cluster acquires a size of 14 atoms, then the 8-member unit with tetrahedral symmetry starts to show up. The 16-atom cluster presents already a 6-atom ring on its surface.

IV. STRUCTURAL PROPERTIES

A convenient way to study local order in condensed systems is by analyzing the pair correlation function $g(r)$.[11] This function is not a directly observed property but is extracted from the structure factor $S(k)$ obtained in diffraction experiments. Several experiments in the past have attempted a measurement of $S(k)$ for various isolated clusters.[14] However, there are no diffraction experiments on silicon clusters to the authors' knowledge. It is interesting though to provide the direct space $g(r)$ in anticipation of experimental evidence. Figure 7 shows $g(r)$ for the neutral 15-atom cluster as obtained from the molecular dynamics simulation of the runs labeled (a) to (f) in Fig. 2(a). This function is calculated from a time average of the number of atom pairs with separation r, $n(r)$, averaged over all r directions, i.e.,

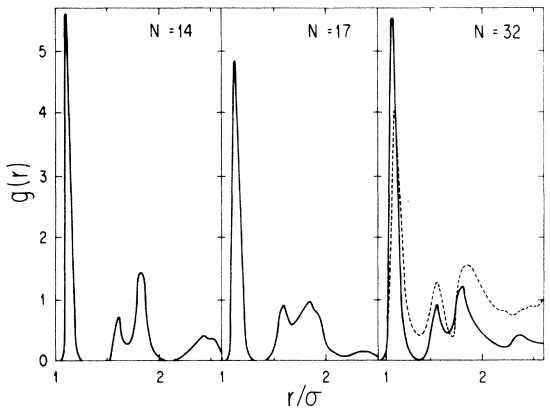

FIG. 8. Pair correlation function at very low temperatures for the neutral 14-, 17-, and 32-atom clusters. For $N = 14$ and 17, $T^* = 0.015$, whereas for $N = 32$, $T^* = 0.006$. The dashed line in the right figure illustrates the inherent pair correlation function of a supercooled liquid as given in Ref. 5.

$$g(r)=n(r)/4\pi r^2\rho_0 \,. \tag{8}$$

Comparison of the low- and high-temperature g provides evidence of the structural rearrangement that occurs when clusters are heated. At low temperatures g is very structured showing, when analyzed versus N, how the coordination shell resolution builds up in the bulk solid (Fig. 8). The high-temperature g could be associated with "droplets," or clusters in the liquid state. However, as no phase transition was resolved from the calculation, it was not possible to find the melting temperature. Therefore, the study of a structural quantity as a function of temperature such as g might be a good candidate for defining a "liquid cluster." The first peak grows broader and lower, when compared to the one at low temperatures. The second coordination shell has almost lost its structure at stage (e) and the gap between first and second coordination shells tends to disappear with increasing T^*. A criterion for having attained a temperature such as to have a droplet might be for instance to calculate the averaged coordination number from $g(r)$, namely

$$n_c(r_{\max})=4\pi\rho_0\int_0^{r_{\max}} r^2 g(r)dr \tag{9}$$

up to $r_{\max}$ equal to the position of the shallow first minimum. Next, select the transition temperature as that temperature where an increase (or decrease) of n_c ($r_{\max}$) takes place. Figure 7 shows this behavior for the 15-atom cluster, since n_c changes by 8% when $T^*=0.063$–0.065. In stage (f), the cluster has melted, the second coordination shell is completely smeared out and the choice of $r_{\max}$ is therefore ambiguous. In Fig. 7(f), right scale and dotted line, the change of n_c versus $r=r_{\max}$ is illustrated. If the same $r_{\max}$ as in the previous stages is chosen, then the coordination number decreases again to 3.2. This behavior is to be expected since the cluster is isolated in the vacuum with no constraints to space expansion. The value of $r_{\max}$ can be associated to a mean Si–Si bond length two silicon atoms are bonded if their interatomic distance is $\leq$ than $r_{\max}$.

Interestingly, the g as a function of N and at very low temperatures carries over to the "inherent" pair correlation function[5] in the slightly supercooled melt of bulk silicon. The latter, as given in Ref. 5, is reproduced by the dotted line in Fig. 8(c). This "inherent" g is the result of mapping the 216-atom system configurations onto nearby potential energy minima. The seeds to build up those minimum-energy configurations seem to be already present in the smaller clusters analyzed in this study.

Other structural correlations might further illuminate the existence of droplets. With this in mind, let's define a "bond angle" as the angle between two bonds converging on the same atom. The bond length can be extracted from $g(r)$ as the value of $r_{\max}$, or alternatively be fixed at $r^*=1.4$, the value where the g deep first minimum lies at very low temperatures. This criterion was used here to be consistent with the previous discussion of bond statistics concerning Figs. 3 to 6. The density distribution of bond angles can be calculated as a function of temperature.

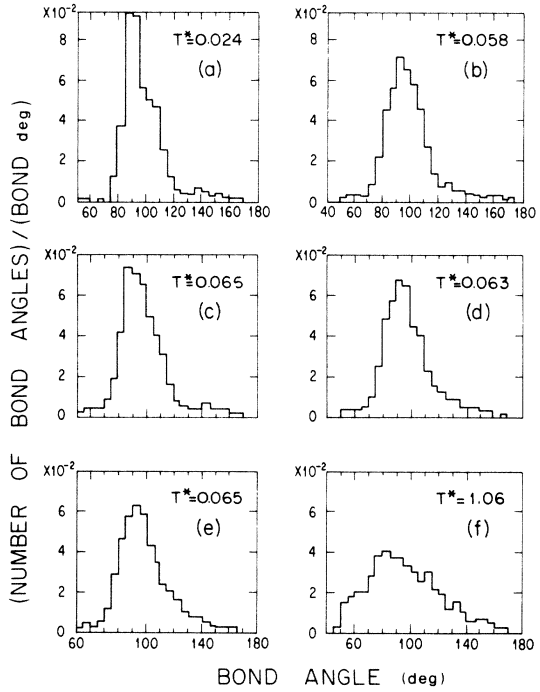

FIG. 9. Density distribution of bond angles in the neutral 15-atom cluster for each of the six temperature steps labeled (a) through (f) in Fig. 2(a). The distribution is normalized to give the number of bonds in the cluster.

Figure 9 shows the smearing of this distribution for the 15-atom cluster as a function of temperature. The different states (a) through (e) correspond to the states shown in Fig. 2(a). Since the smearing starts to show up at $T^*\sim 0.07$, this temperature can be identified as the melting temperature. The elapsed time between successive collection of angles was 0.5τ and 30 configurations were used in the averages. Finally, Fig. 10 illustrates how the density distribution of bond angles builds up as a function of N toward the bulk values.

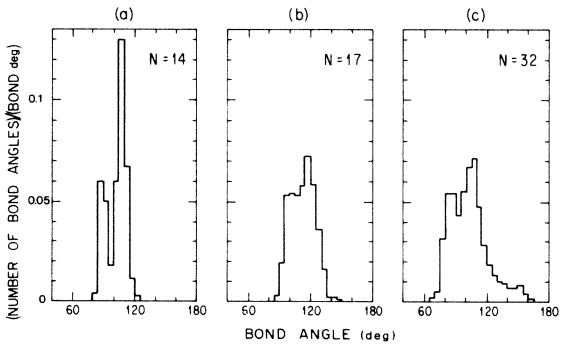

FIG. 10. Density distribution of bond angles at very low temperatures for the neutral 14-, 17-, and 32-atom clusters. The distribution is normalized to give the number of bonds in the cluster. (a) and (b), $T^*=0.015$; (c), $T^*=0.006$.

V. CONCLUSION

The behavior of the Stillinger and Weber potential model was examined in the process of building up a sequence of isolated cluster growth. This model has successfully given many of the silicon bulk properties. It is important to have now the results of the early stages of aggregation using this silicon model to complete the description of the condensed phases of that material. Further improvements on the choice of the potential parameters are certainly possible, as suggested in Ref. 5. The results of this study give more information that can lead to a better set of parameter values, especially of ε if the experimental cohesive energy of the more abundant neutral clusters were known.

Several new conclusions emerge from this study. First, model potentials of covalent materials should have parameters fitted not only on bulk properties but also on properties of small clusters containing less or enough atoms to fill the first coordination shell. Second, the clusters found in the early stages of growth do not have locally the point symmetry of the more stable bulk crystal. Instead, it seems that the underlying structure of the liquid (as obtained in Ref. 5) dominates the process of growth. Third, it is clear that using the same potential model neutral and positively charged clusters aggregate differently. The neutral sequence shows a high stability for 10- and 14-atom clusters, whereas the charged sequence yields 13 and 15. The sequences of growth determined in this simulation experiment were produced in the same way that the bulk crystal would be produced. However, it cannot be excluded that other growth sequences obtained by other quenching methods could better simulate the formation of amorphous clusters.[15] The identification of the clusters here with "real clusters" will demand a more exact knowledge of the various growth parameters used in the laboratory.

ACKNOWLEDGMENTS

We gratefully acknowledge many valuable discussions with Professor Dr. T. P. Martin. This research was supported by a joint Consejo Nacional de Ciencia y Tecnología, México (CONACyT)—Centre National de la Recherche Scientifique, France (CNRS) Contract and under CONACyT Grant No. PCCBBNA-022643. Laboratoire de Physique Théorique et Hautes Energies is a "Laboratoire associé au CNRS."

[1]J. M. Ziman, *Models of Disorder* (Cambridge University Press, Cambridge, 1979), Chap. 2 and references therein.

[2]D. E. Polk, J. Non-Cryst. Solids **5**, 365 (1971); D. Henderson, *ibid.* **16**, 317 (1974); J. C. Philips, *ibid.* **43**, 37 (1981); L. Guttman, Phys. Rev. B **23**, 1866 (1981); F. Wooten, K. Winer, and D. Weaire, Phys. Rev. Lett. **54**, 1392 (1985).

[3]F. H. Stillinger and T. A. Weber, Kinam **3A**, 159 (1981); Phys. Rev. A **25**, 978 (1982).

[4]P. N. Keating, Phys. Rev. **145**, 637 (1966); T. Takai, T. Halicioglu, and W. A. Tiller, Scr. Metall. **19**, 709 (1985); R. Biswas and D. R. Hamann, Phys. Rev. Lett. **55**, 2001 (1985); J. Tersoff, *ibid.* **56**, 632 (1986); S. Saito, S. Ohnishi, and S. Sugano, Phys. Rev. B **33**, 7036 (1986).

[5]F. H. Stillinger and T. A. Weber, Phys. Rev. B **31**, 5262 (1985).

[6]L. A. Bloomfield, R. R. Freeman, and W. L. Brown, Phys. Rev. Lett. **54**, 2246 (1985); L. A. Bloomfield, M. E. Gewsic, R. R. Freeman, and W. L. Brown, Chem. Phys. Lett. **121**, 33 (1985).

[7]T. P. Martin and H. Schaber, J. Chem. Phys. **83**, 855 (1985).

[8]L. Verlet, Phys. Rev. **159**, 98 (1967).

[9]R. R. Teachout and R. T. Pack, At. Data **3**, 195 (1971).

[10]C. L. Brian and J. J. Burton, J. Chem. Phys. **63**, 2045 (1975).

[11]E. Blaisten-Barojas and H. C. Andersen, Surf. Sci. **156**, 548 (1985); E. Blaisten-Barojas, Kinam **6A**, 71 (1984).

[12]T. P. Martin (private communication).

[13]J. Tagüeña-Martínez, L. E. Sansores, and E. A. Cetina, Phys. Rev. B **27**, 2437 (1982).

[14]J. Farges, M. F. de Feraudy, B. Raoult, and G. Torchet, Surf. Sci. **106**, 95 (1981); J. Chem. Phys. **78**, 5067 (1983); S. S. Kim and G. D. Stein, J. Colloid Interface Sci. **87**, (1982); J. W. Lee and G. D. Stein, Surf. Sci. **156**, 112 (1985).

[15]M. R. Hoare, Adv. Chem. Phys. **40**, 49 (1979); T. P. Martin, Phys. Rep. **95**, 167 (1983); I. Garzón and E. Blaisten-Barojas, Chem. Phys. Lett. **124**, 84 (1986).